6.2 Influence of Carbon on Helium – Defect Interactions in Single Crystal Iron Following Helium Implantation: Thermal Helium Desorption and Positron Lifetime Measurements and Modeling

— Xunxiang Hu (University of California, Berkeley), Donghua Xu, and Brian D. Wirth (University of Tennessee, Knoxville)

OBJECTIVE

The objective of this work is to identify the kinetics and energetics of helium-point defect interactions of helium implanted single-crystalline iron.

SUMMARY

The thermal desorption spectra of helium from single crystalline iron samples was obtained as a function of implantation conditions using the Berkeley thermal helium desorption spectroscopy (THDS). The implantation conditions were He ion implantation energies of 10, 20, or 40 keV at a consistent dose level $1x10^{15}$ He/cm^2. Constant rate heating ramps were employed to thermally desorb the implanted helium. The present results, in which the single crystalline iron has a lower carbon content, indicate a significant effect of carbon on the helium desorption behavior, when compared to our previous measurements. The results indicate that major helium releasing peaks of the iron samples with higher purity show up at lower temperatures. A spatially dependent cluster dynamics model is utilized to reproduce the helium spectrum in BCC region. Meanwhile it provides an opportunity to optimize the basic thermodynamic and kinetic energy parameters of helium and small helium-vacancy clusters. The combination of the modeling and THDS measurement allows identification of possible mechanisms (e.g. shrinkage of He_3V_2) responsible for the measured helium desorption peaks. Furthermore, the model is also used to predict the depth dependence of helium and helium-defect clusters as a function of time and temperature during the THDS measurement. The samples with the implantation condition of 40 keV, $1x10^{15}$ He/cm^2 have been measured by positron annihilation spectroscopy, as an initial attempt to correlate a second experimental technique of the vacancy cluster population against the modeling predictions. Good agreement is obtained between the positron lifetime analysis and the modeling calculation. The recent work provided an overview of the self-consistency of the model predictions based on the assumptions made in the helium-point defect binding and interaction energies and diffusivities.

PROGRESS AND STATUS

Introduction

A large quantity of helium will be generated in fusion structural materials (e.g. ferritic/martensitic steel) as a result of direct implantation or transmutation reactions induced by the large 14 MeV peaked neutron spectrum [1-3]. Since helium has extremely low solubility in most metallic alloys, it has a strong tendency to cluster with various types of defects and to precipitate out as bubbles. It has been observed that the production of helium in typical engineering alloys can lead to significant property degradation, such as hardening, fast creep rupture, swelling and embrittlement [1-4]. Therefore, studying helium effects on the microstructure and mechanical properties is of tremendous importance in fusion materials research. Since the macroscopic properties

are determined by the microstructure and microscopic interactions, a major task of this study is to understand the helium effects by uncovering the mechanisms by which helium migrate and interact with various types of defects, and by which the interactions govern the subsequent nano/microstructural evolution in irradiated materials. This is an inherently multi-scale problem spanning from atomistic to macroscopic dimensions in both time and space.

The theoretical foundation of helium behavior was laid in the 1970s and 1980s with concern with mainly about the fission conditions [5-10]. Due to the increasing interest of fusion energy, a resurgence of research activities on helium is witnessed in recent years. BCC iron and ferritic alloys attract most of the concern, particularly. The kinetics, energetics and thermal stability of helium and small helium-containing clusters, and the helium interactions with grain boundaries and dislocations have been studied by atomistic simulations using molecular statics/dynamics and ab inito approaches. Rate theory models are also developed by different researchers to simulate the evolution of helium-defect clusters and fit the experimental results. Meanwhile, experiments using optical or electron microscopy, nuclear reaction depth profiling, positron annihilation spectroscopy, thermal helium desorption spectrometry and other techniques have been executed to analyze the behavior of helium and helium-containing clusters in BCC iron and ferritic alloys [11-16]. However, the overall picture of helium in BCC iron or ferritic alloys remains incomplete and not yet self-consistent. On one hand, there are still significant open questions such as the energetics of large He-V clusters. On the other hand, apparent discrepancies still exist in the literature regarding some basic subjects, such are the binding energy of HeV cluster.

A newly developed, parallel computer code for modeling the spatially-dependent cluster dynamics of helium, vacancy and interstitial clusters has been used to predict the earlier THDS experimental results in our research group [17,18]. A good agreement could be obtained by optimizing the values for the migration energy of single vacancy and the binding energies of small He-V clusters. These results were explained by invoking the presence of impurities in the experimental samples, which were not taken into account in the initial model. Since carbon is a common impurity in iron and since it strongly interacts with vacancies, as confirmed by ab initio calculation [19,20], carbon was proposed as the most likely candidate for the effect observed.

In this work, we conducted THDS measurements for the new batch of single crystalline irons implanted with 10keV, 20keV, 40keV to a constant dose $1x10^{15}$ He/cm^2. The comparison between the new helium desorption spectrum and the previous results of old samples give us a general picture of how the carbon's presence affects the helium outward flux. The cluster dynamic model is incorporated to fit the helium desorption spectrum and analyze the He-V clusters' evolution. The model's prediction will be verified by positron annihilation spectroscopy (PAS) measurements at selected annealing conditions of interest. This report will provide an overview of the self-consistency of the model predictions based on the assumptions made in terms of the He-point defect binding and interaction energies, and diffusivities.

Experimental Procedure

Two different batches of single crystalline irons were used in this project. The old samples with a purity of 99.94% were provided by Dr. S. A. Maloy at Los Alamos

National Lab. The new bacth of high purity (99.98%) single crystalline iron plates of 1mm in thickness, 4.5mm in diameter were purchased from Goodfellow. Before measurements, the samples were mechanically polished to 1 μm grade smoothness, and then commercially implanted at room temperature with He-4 ions.

Partial helium current was measured in Berkeley ultrahigh vacuum (~10^{-10} torr) thermal desorption system as a function of temperature during constant ramp rate (1 K/s) from room temperature up to 1300°C. The helium current was then converted to the instantaneous desorption rate by multiplying a proportionality coefficient, determined separately with a calibration procedure. More details of our system can be found in Ref. 21 and 22.

RESULTS

In order to study the effect of impurities, chemical analysis was conducted for both batches by Luvak Inc. to identify the compositions of samples. The following table shows the analysis details. No other elements were detected in excess of 0.01%.

Table 1. Composition of the two batches of single crystalline irons

	Carbon	Copper	Manganese	Nickel	Iron
Old samples	0.023%	< 0.01%	0.01%	< 0.01%	Balance
New samples	0.007%	0.0385%	0.049%	0.0135%	Balance

The analysis results indicate that carbon content of the old samples is three times more than that of new samples while the other impurities, such as Cu, Mg and Ni, of old samples are less than those present in the new samples. The substitutional solutes of copper, nickel and manganese should have very little impact on the binding energies of He-V clusters because of their similar properties (e.g. atom size) as iron. In contrast, carbon has a strong tendency to interact with vacancies, as confirmed by ab initio calculations. In this paper, we will focus on the effect of carbon on the helium desorption spectra. In the following, when the high purity of SC samples are mentioned, it represents the new samples with low carbon content; when low purity of SC samples are used, it means the old samples with relatively higher carbon content.

The facility experienced the change of tungsten crucible recently. A new tungsten crucible welded by a supporting tantalum rod replaced the separated ones used before. The new design will guarantee the stability of the thermal couple in the measurement in order to provide more accurate temperature control. Meanwhile, the facility accepted the new components after several runs. A relatively cleaner background was obtained whose helium current remains in the small region of low values, 1.4×10^{-13} A~3.2×10^{-13} A.

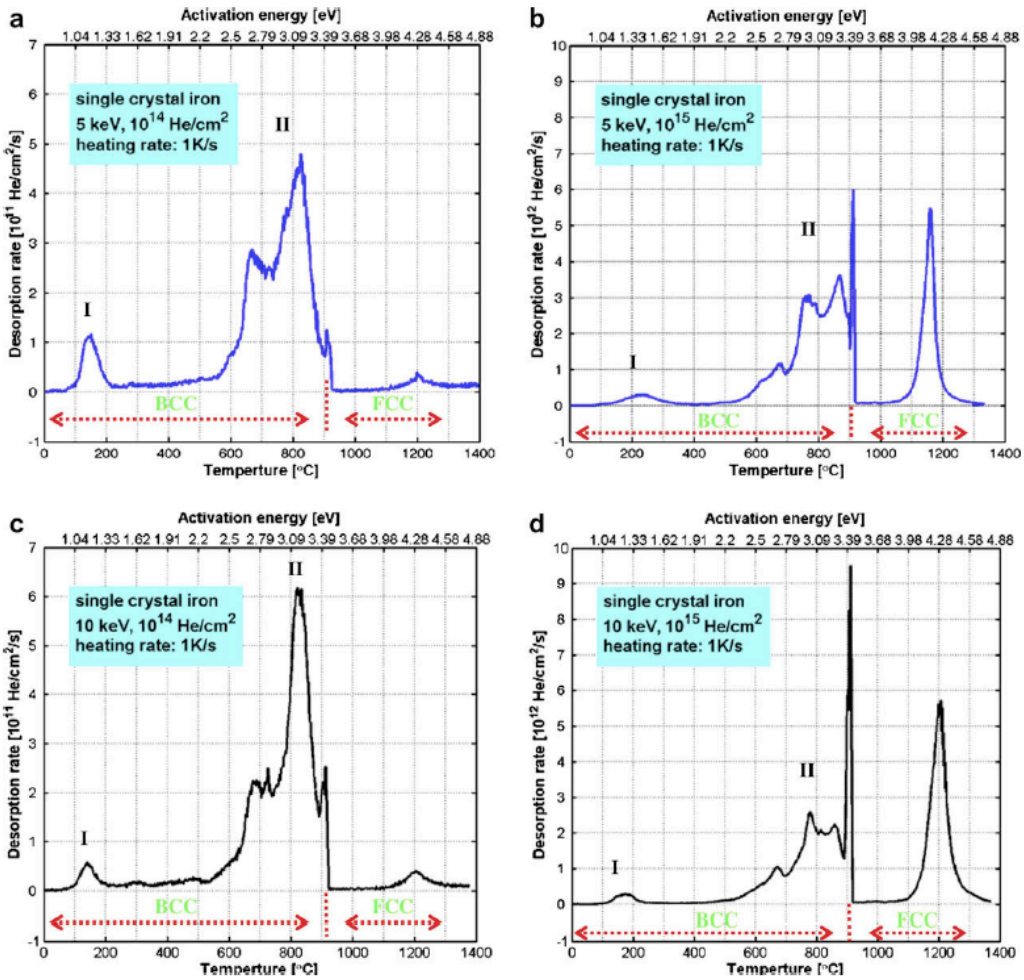

Fig.1 [22]. Desorption spectra of low purity single-crystalline iron implanted with ^{4}He at: (a) 5keV, 1x10^{14} He/cm^2; (b) 5keV, 1x10^{15} He/cm^2; (c) 10keV, 1x10^{14} He/cm^2; (d) 10keV, 1x10^{15} He/cm^2.

General features of low purity SC spectra

Fig.1 presents experimentally obtained thermal helium desorption spectra for the low purity single crystalline iron samples, which were implanted with either 5 or 10keV He ions to a fluence of 10^{14} or 10^{15} He/cm^2, during thermal annealing with a constant heating rate of 1°C/s. The data clearly show two well separated major desorption groups within the BCC temperature range (up to 912°C, where the appearance of the sharp peak marks the alpha-gamma phase transformation of iron): Group I below ~300°C and Group II from ~550°C to 912°C. Major helium releasing region is above 600°C. Further, increasing implantation fluence greatly enhances the fraction of retained helium that will not desorb until ~1200°C. The energy's difference dose not show significant discrepancy in the helium desorption spectra compared to the fluence's effect.

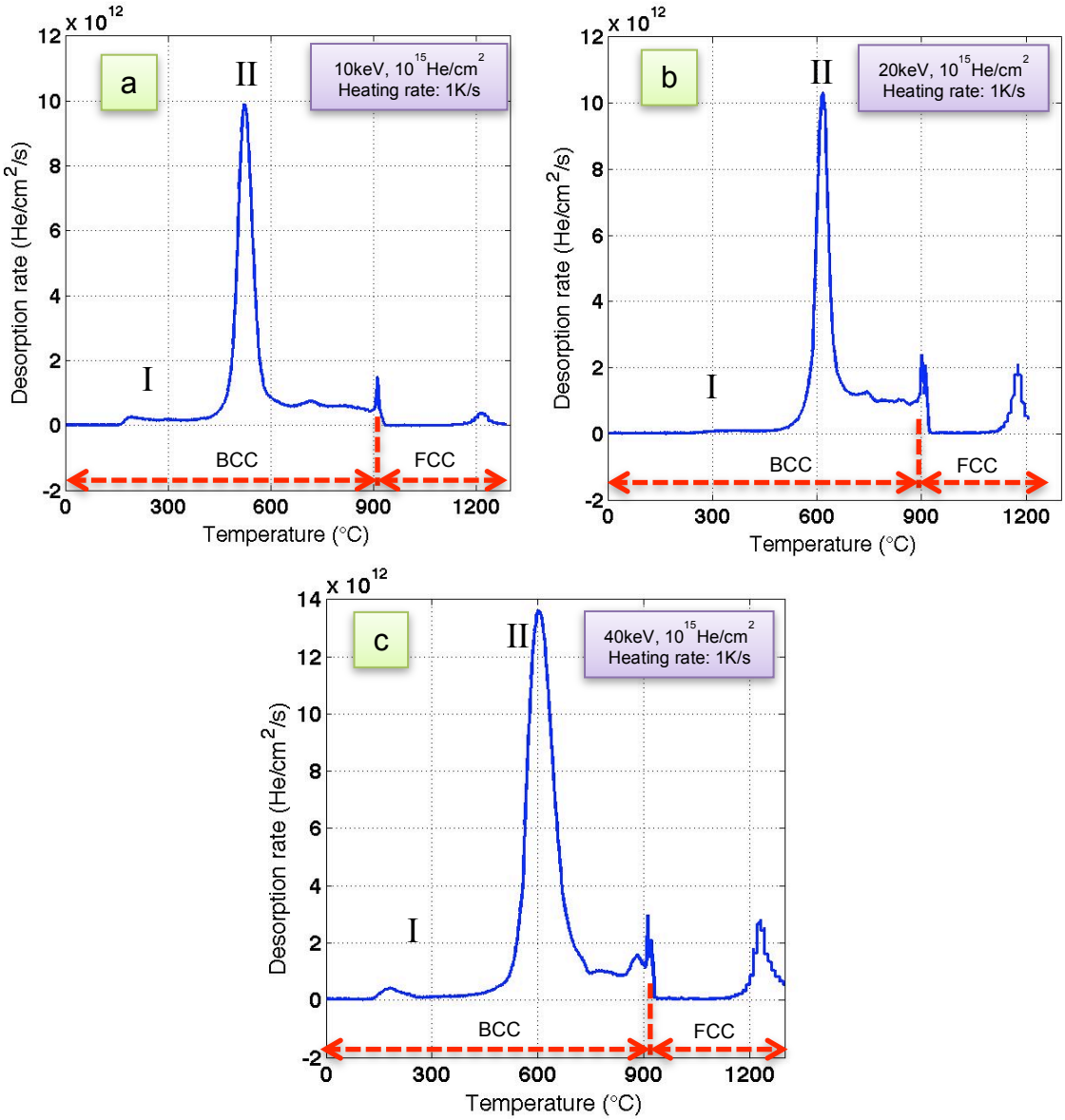

Fig. 2. Desorption spectra of high purity single-crystalline iron implanted with ^{4}He at: (a) 10keV, 1x10^{15} He/cm^2; (b) 20keV, 1x10^{15} He/cm^2; (c) 40keV, 1x10^{15} He/cm^2.

General features of high purity SC spectra

The helium desorption spectra obtained from high purity SC samples (new samples) for the three combination of implantation conditions used in the latest measurement are presented in Fig.2(a)-(c). There also exists a sharp peak for each of the spectra, which is also observed for other experimental conditions. In Ref. 21, it shows the strong evidence leading to the conclusion that this peak is primarily due to the alpha-gamma (BCC-FCC) phase transformation. Therefore, in this work, as what we did before, this peak is used to calibrate the temperature reading by setting this peak position to 912°C (the well known value of BCC-FCC phase transformation in pure iron) and utilizing a linear-correction to the other temperature values.

The new spectra also involve the existence of multiple helium release groups: Group I below ~300°C and Group II from ~450°C to 912°C. The group I here is similar to that in old spectra, although Fig.2(b) dose not show the obvious release peak around 200°C. In group II, a significantly large peak shows up around 600°C in the BCC region, which is not observed in the old spectra. From low implantation energy to higher implantation energy, the big peak switches to a position of higher temperature. Also, after the concentrated helium release in this big peak, a plateau with small fluctuations continues up to the phase transformation point. In Fig.2(c), there is an obvious peak in the plateau just before the BCC-FCC transformation. The other similar feature is that the retained helium will not be desorbed until ~1200°C. The Group II, major helium desorption region, starts from a lower temperature point (~450°C) compared to the old spectra. In general, the helium spectra of high purity SC look like more concise and less diffuse than old spectra of low purity SC.

It is reasonable to ascribe the less diffuse feature of the high purity SC spectra to the lower concentration of carbon. As mentioned earlier, the most crucial distinctions are the carbon content in the samples while the other impurities' effect can be neglected due to their substitutional positions. Carbon is known to affect the migration of self-defects in alpha iron, particularly vacancies. Some researchers [23,24] have pointed out that the effective migration energy of vacancies in BCC iron measured experimentally varies between 0.6 to 1.5 eV with higher values for specimens with higher carbon content. Some of these observations have been explained with the help of density functional theory calculations. Experiments also provide the evidence of the formation of various carbon-defect complexes, in particular carbon-vacancy clusters [25]. These can explain our experimental results from a very straight-forward point of view and approve our assumption that helium will be desorbed in a lower temperature range for the specimens with high purity due to the smaller effect of carbon.

However, how the energetics of helium and helium-vacancy clusters change cannot be seen clearly only by the experiment. Thus we next describe the use our spatially-dependent cluster dynamics code to model the new helium spectra and compare the energies applied here to the previous simulations. This will provide an overview of the energetic changes in detail.

Spatially-dependent Cluster Dynamics Model

Despite substantial effort, the overall picture of helium in BCC iron or ferritic alloys remains disconnected, incomplete and not yet self-consistent. A model that incorporates both temporally and spatially depent He and point defect diffusion, trapping and de-trapping kinetics during the implantation process and thermal annealing has been developed in our research group. The detailed ideas of this model can be found in Ref.17 and 18.

As shown in the Ref.17 and 18, the modeled desorption spectra can result in good overall agreement with the experiments by optimizing the parameters for the vacancy migration energy and the binding energy of very small helium-vacany clusters containing one to three vacancies and up to five helium atoms. The selection of optimized parameters has been guided from input from ab initio calculations, as well as from molecular dynamics and cluster dynamics simulation results.

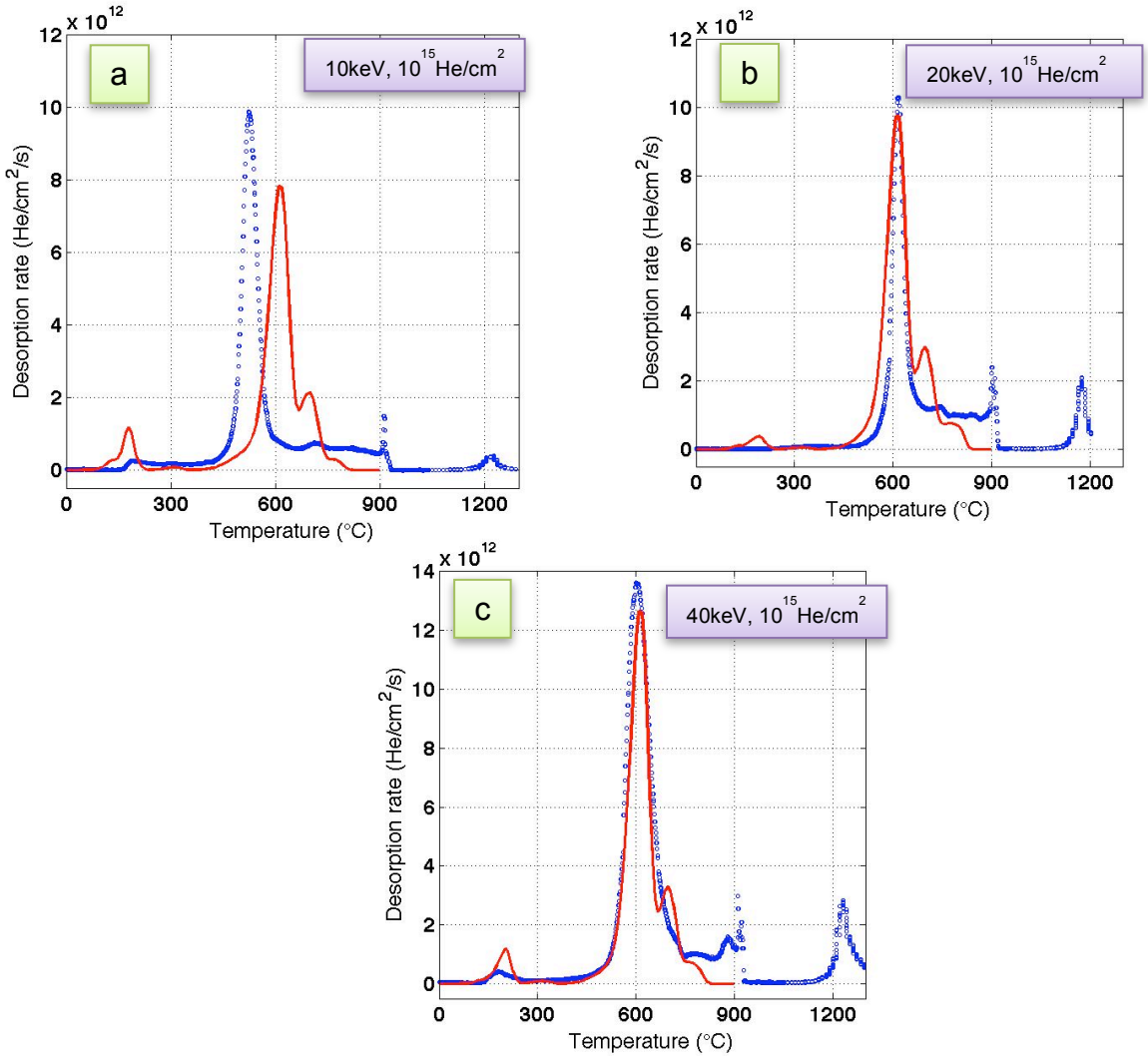

Fig.3. Experimental (open symbols) and predicted (solid lines) He desorption spectra in single crystalline iron of high purity following implantation of (a) 10keV, $1x10^{15}$ He/cm^2; (b) 20keV, $1x10^{15}$ He/cm^2; (c) 40keV, $1x10^{15}$ He/cm^2.

New Modeling Results

The new helium desorption spectra provides another opportunity to show the self-consistency of the code. A parameter optimization was performed, which is aimed at improving the agreement between the model and the experiments. The sold red lines in Fig. 3 represent the predicted desorption spectra with the best overall agreement with the experiments obtained so far using a different set of optimized parameters from previous model for low purity SC samples.

As shown in Fig.3, quite similar to the experimental spectra, the model reproduce the two well separated major desorption groups within the BCC temperature range, one below 300°C and the other above 450°C. Moreover, the small peaks in Group I are predicted well with a good position overlap. Although the model successfully generate

the big peaks in Group II, the position for it in Fig. 3(a) does not fit the experimental result very well, shifting to the higher temperature region; while for Fig. 3(b), (c), the big peaks' positions are well produced. The other unfavorable aspect is that the plateau in the experimental spectra was not seen in the model prediction. Snuggling up to the big peaks in the modeled curves, a small peak show up and then helium desorption rate decreases abruptly. Furthermore, the model requires further improvement or optimization to better reproduce the intensities of the desorption peaks, the major peak's position for the lower implantation energy specimen as well as the plateau within Group II.

Influence of Carbon Existence on the Energetics and Kinetics

In our simulation, the migration energy of single vacancy is optimized to be the value of 0.82eV which is smaller than that used for the model of low purity samples. In the table 2, the major binding energies of helium for some important clusters are listed. It is very clear that the binding energies of the important clusters for modeling high purity samples are smaller than that for modeling low purity samples, except the value for the helium binding energy of He_2V. This situation has agreed with our experimental results and analysis. The other thing that should be mentioned is that all of the energies applied in the model are within the energy range computed by ab initio, molecular dynamics and thermodynamic.

Carbon's existence become a fetter for the mobility of helium and other mobile small clusters and induce the binding energies of helium-vacancy clusters to shift to higher values. A recent rate theory modeling work indicate that the explicit inclusion of a few small carbon-containing clusters $He_nV_mC_p$ (n,m,p=0,1,2) along with ab initio vacancy migration energy is shown to produce similar agreement with experiments to that obtained by an effective but larger vacancy migration energy without considering carbon.

Table 2. Comparison of the binding energies (eV) of helium for small He-V clusters.

Clusters	High purity	Low purity	Ab initio	MD	Thermodynamic
HeV	2.56	3.20	2.3	3.7	3.39
He_2V_2	2.98	3.17	2.75	3.8	3.17
He_2V	1.13	1.12	1.84	2.19	1.72
He_3V_2	2.25	2.45	2.07	2.81	2.29
He_4V_2	1.10	1.18	2.36	2.48	1.43
He_5V_3	1.70	2.17	n/a	3.11	1.92

Possible Mechanisms Responsible for He Desorption Peaks

The combination of the modeling and thermal desorption measurements allows identification of possible mechanisms governing helium desorption peaks. Actually, when we do the optimization of the binding energies of small clusters to fit the experimental results, the cluster distributions at different temperatures have been analyzed.

The case of high purity samples implanted by 40keV, $1x10^{15}$ He/cm^2 is taken as an example. The shrinkage of He_2V is responsible for the helium desorption peak in Group

I. The production of the big helium release peak derives from the large decrease of three small clusters, HeV, He_2V_2 and He_3V_2; the peak close to the major one within BCC region is due to dissociation of HeV. These are also our foundation to do the parameter optimization.

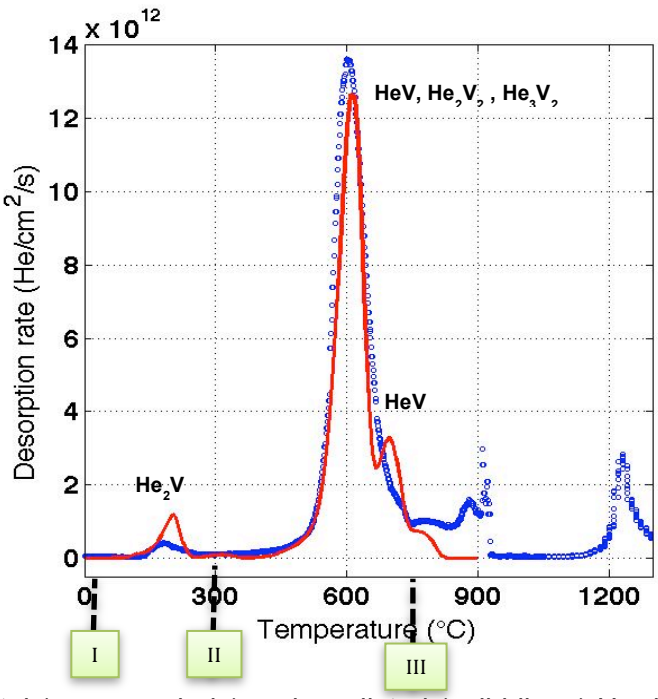

Fig.4. Experimental (open symbols) and predicted (solid lines) He desorption spectra in single crystalline iron of high purity following implantation of 40keV, $1x10^{15}$ He/cm^2; Major shrinkage of small clusters are labeled nearby the corresponding He desorption peaks; Three points of interest are marked to do the positron lifetime analysis.

Cluster Evolution Predicted by Model

While some small clusters listed above with optimized binding energies are important species to accurately model the desorption spectra, they are not the whole story. In fact, helium release is intimately coupled to the overall clusters evolution dynamics and each desorption group involves a collective action of a distribution of cluster size.

Here we picked up three interesting points covering the two major helium desorption groups within BCC region, as marked in Fig. 4, which are: I after irradiation, II at 300°C, III at 750°C.

In the model, we can obtain the cluster area concentration for various types of clusters along the depth of the sample at different temperatures. For the selected three points, the cluster concentrations come from the integration along the depth at each picked point. Fig.5 shows the cluster distribution.

From the calculation, the helium-vacancy cluster distribution is shown clearly. After irradiation by He-4, the clusters with vacancy number of 1~7 and helium number of 1~4 exist inside the sample where He_2V and HeV dominate the distribution. At point II after the first helium desorption peak, HeV occupies 75% of the total cluster concentration and the number of vacancy and helium in the cluster are 1~9 and 1~7, respectively. The clusters experience some significant changes after the second group of helium release peaks. At the third point, although HeV is still dominating, the size of the He-V clusters grow a lot with the helium number to be 24 and vacancy number up to be 18.

The change of the amount of helium-vacancy clusters can be seen clearly in the figure. The inclusion of clusters increases first because of the stronger mobility of helium and single vacancy, and then decreases due to helium desorption and recombination of interstitials and vacancies.

In the Ref.18, more simulating results of the cluster evolution for lower implantation fluence and higher implantation fluence are discussed. However, all of these predictions should be verified by transmission electron microscopy and/or positron annihilation spectroscopy measurements.

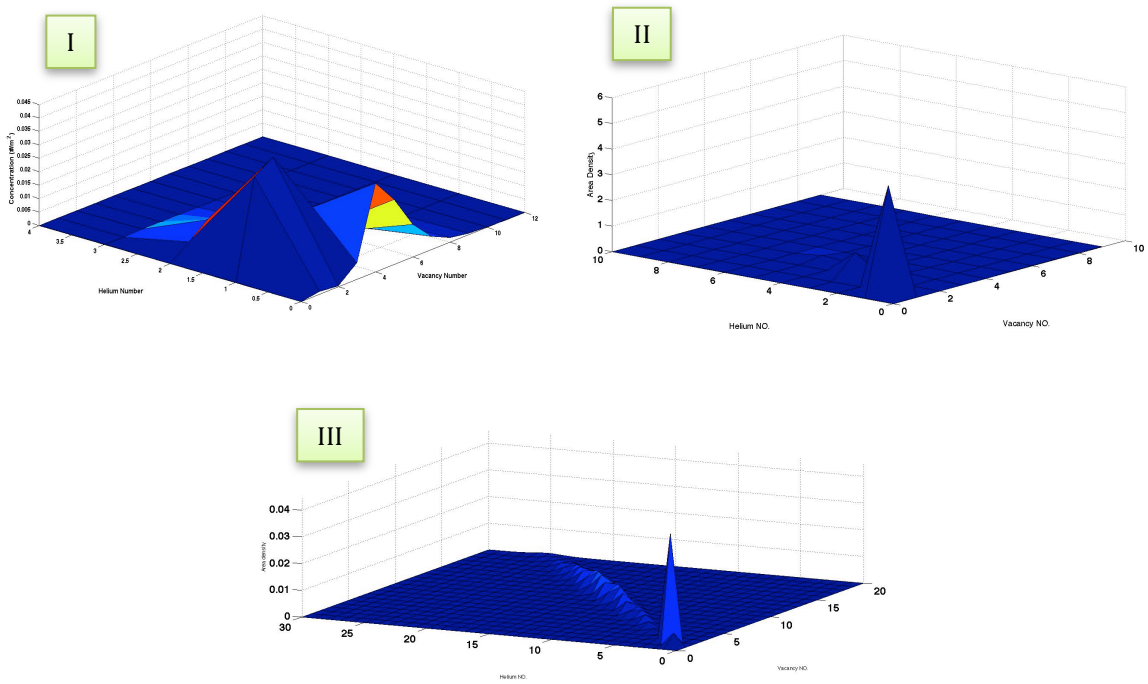

Fig. 5. Computed cluster distribution for the three selected points: I after irradiation, II at 300°C, III at 750°C.

Positron Annihilation Spectroscopy (PAS) Measurements

The use of positron annihilation spectroscopy for studies of defects in solids is mainly based on two facts. The first one is that positron may annihilate with an electron

accompanying the emission of two gamma radiation who have the equivalent energy to the two particles. The second fact is that positrons injected into a material will become trapped in defects and annihilate there. By suitable measurements of the emitted gamma quanta, it is then possible to obtain useful information about the characteristics of those defects that trap positrons [26].

The positron lifetime measurements were conducted at room temperature on the Berkeley positron annihilation spectroscopy facility. Because the conventional sample-source-sample sandwich geometry was employed, an identical irradiation was given to both of the samples. The source was made from a ^{22}NaCl solution evaporated onto the surface of the samples.

The high purity SC iron samples in the implantation condition of 40keV, $1x10^{15}$ He/cm^2 were selected and two interesting points, labeled in Fig.4 are picked to do the annealing processes and PAS measurements. The annealing was performed in an ultra high vacuum environment used for THDS measurement, increasing the temperature to the set values with a heating rate of 1K/s which is the same with THDS in order to verify the cluster evolution mentioned before.

The data were analyzed by resolving two exponentials, which gave a satisfactory fit. Fig.6 shows the parameters of the lifetime spectra for the high purity SC iron as functions of the annealing temperature. As can be seen from this figure, the long lifetime, τ_2, decreases from 231ps to 214ps for the irradiation condition and 300°C annealing process; then it increases from 214ps to 278ps for the two annealing conditions, 300°C to 750°C. We can transfer the long lifetimes to the information of cluster size by comparing them to the Fig. 3 and Fig. 4 in Ref.27. The two figures show the positron lifetimes in vacancy clusters and helium-vacancy clusters in BCC iron. In our case, the positron lifetime of 231ps after irradiation represents the existence of small clusters, while the positron lifetimes in pure vacancy cluster V_4 and in helium-vacancy cluster HeV_6 are around this value of 231ps. Since it will not only one type of specie, the measured positron lifetime is a collective result. Based on this info, we can justify that the small cluster with the helium number up to 4 and vacancy number up to 8 present, conservatively. At the annealing point of 300°C, the lifetime is 213ps corresponding to V_2 or HeV_5 which means that small clusters still dominate and no large helium-vacancy cluster show up. The long lifetime for the condition of annealing at 750°C is 278ps aiming at the existence of V_{10} and/or He_2V_m(m>10). These results perfectly agree with our modeling calculations. For the mean lifetime indicated on the left in Fig.6, it has a decreasing tendency .

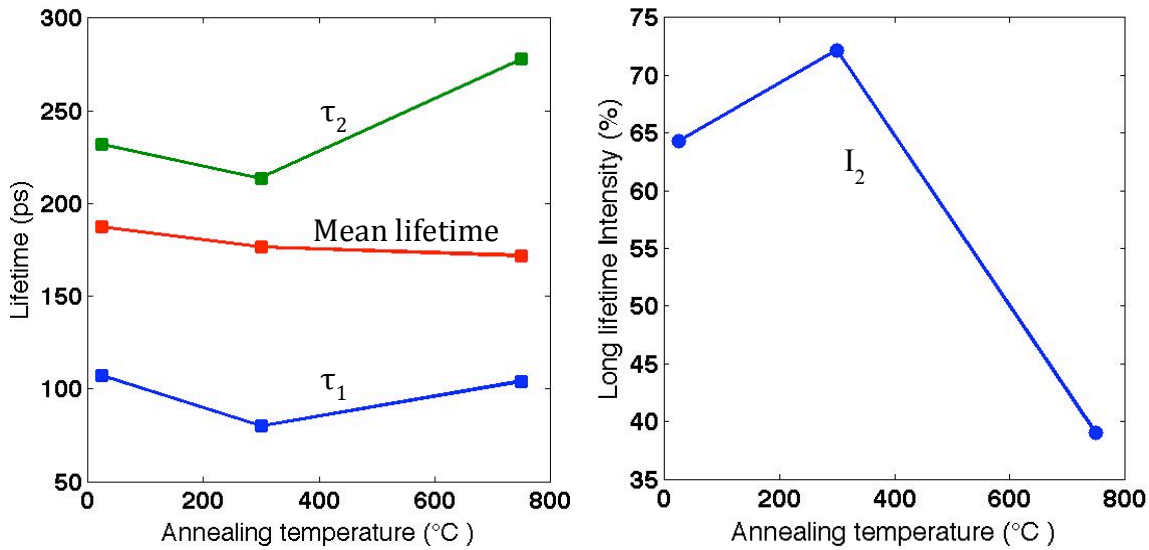

Fig.6. Two components analysis of the positron annihilation lifetime spectrum after each step of the annealing for the high purity SC irons implanted by He-4 of 40keV, $1x10^{15}$ He/cm^2.

The other important parameter is the intensity of the long positron lifetime. The intensity corresponds to the density of vacancy clusters. As shown in Fig.6, the intensity increases from 64.3% to 72.2% and then reduces to 39%. From the initial point to the 300°C annealing condition, the helium concentration grows because helium and single vacancy move fast and combine together to form helium-vacancy clusters with the temperature increasing. At this time, the helium release rate is not comparable to the formation of helium-vacancy clusters. For the 750°C annealing condition, it is located in the Group II region just after the major helium desorption. The retained helium is much less than initial condition. At this high temperature, the mobility of vacancy, helium and other small cluster is intense. The recombination of interstitials and vacancies will also induce the reduction of the clusters. These observations verify our model results in another way.

A Tentative Method to Compute the Overall Positron Lifetime

From the model calculations, we can obtain the detailed cluster distribution which can be compared to the information brought by the long positron lifetime. However, is there a straightforward way to predict the positron lifetime based on the model results?

Here, a tentative and rough method was conducted to combine the modeled helium-vacancy cluster distribution and the theoretical positron lifetime. The theoretical positron lifetime for various size of clusters are from the Fig. 3 and Fig. 4 in Ref. 27 directly or by interpolation. When the He-V cluster is big enough (e.g. He_mV_n , m>24, n>15), we assume that the positron lifetime is saturated, at a value of 308ps.

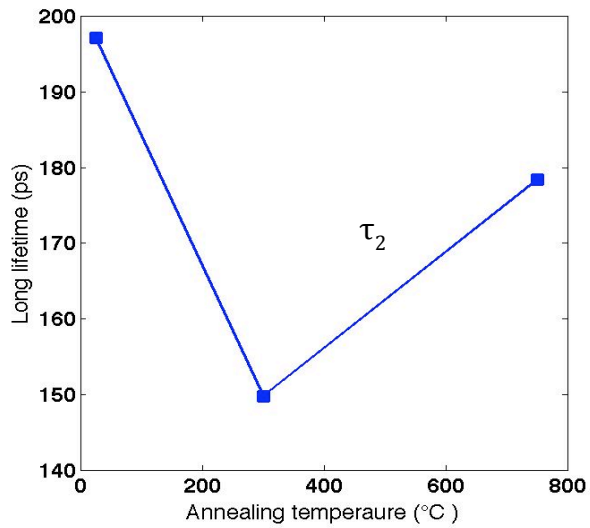

Fig.7. Calculated positron long lifetime for the three selected points.

The contribution of different clusters is based on their density fraction of the total cluster concentration. Then the contribution of each cluster shown in the model result is multiplied by the related lifetime. The sum of all of the computed values is considered the collective positron long lifetime in the defect region.

Although the method is simple, it can give a much more straightforward view of how the long lifetime of positron changes at different annealing stages. Fig.7 indicates the predicted results. As shown in the figure, the long lifetime decreases from 197ps to 149ps for the two stages of after irradiation and annealing at 300°C; then it goes up from 140ps to 178ps for the two annealing stages. The basic tendency of the curve is consistent with the experimental results. The disappointment is that the model underestimates the values of the positron lifetime and the increase value from I to II is larger than that from II to III, because the model method to calculate lifetime is simple and the samples used in the experiments are not ideally pure while some other defects exist, such as dislocations, small voids, etc. Furthermore, we are trying to develop a better way to model the measurements.

CONCLUSION

The impurities (carbon) effect on the helium desorption spectra was analyzed in details by comparing different batches of samples. The results show that the implanted helium will be released earlier for high purity single crystalline irons without more carbon's fetter. A spatially dependent cluster dynamics model is applied to reproduce the spectra which gives a overview of how the binding energies of small clusters and migration energy of vacancy change. The comparison shows that they are smaller for the high purity irons. Moreover, positron lifetime measurements are conducted for the high purity specimens at a selected implantation condition, of 40keV, $1x10^{15}$ He/cm^2. Three points were picked up to do the measurement, after irradiation, annealing at 300°C and annealing at 750°C. The PAS measurements are compared to the modeled cluster distribution at each stage. A good agreement shows up to prove the self-consistency of the model. Furthermore, a

simple method to calculate the positron lifetime for different stages is indicated here and not bad results were obtained.

As to the future work, more efforts are necessary to study the impurity effects by both experiments and models. A more advanced model with He-V-C complex should be developed. For the PAS experiment and simulation, additional implantation conditions and more reliable modeling method are needed. Meanwhile, the combination of neutron irradiation and helium implantation should be done to push the research toward to the more real fusion environment.

REFERENCES

[1] H. Ullmaier, *Nucl. Fusion* **24** (1984) 1039.
[2] L. K. Mansur, M. L. Grossbeck, *J. Nucl. Mater.* **155** (1988) 130.
[3] L. K. Mansur, W. A. Coghlan, *J. Nucl. Mater.* **119** (1983) 1.
[4] H.Trinkaus, B. N. Singh, J. *Nucl. Mater.* **323** (2003) 229.
[5] K. C. Russell, *Acta Metall.* **20** (1972) 899.
[6] K. C. Russell, *Acta Metall.* **26** (1978) 1615.
[7] H. Trinkaus, *Rad. Eff. Defects in Solids* **78** (1983) 189.
[8] L. K. Mansur, E. H. Lee, P. J. Maziasz, A. P. Rowcliffe, *J. Nucl. Mater.* **141-143** (1986) 633.
[9] N. M. Ghoniem, S. Shafafat, J. M. Williams, L. K. Mansur, *J. Nucl. Mater.* **117** (1983) 96.
[10] R. E. Stoller and G. R. Odette, *J. Nucl. Mater.* **131** (1985) 118
[11] M. B. Lewis, K. Farrell, *Nucl. Instrum. Meth. Phys. Res. B* **16** (1986) 163.
[12] K. Ono, et al., J. *Nucl. Mater.* **329–333** (2004) 933.
[13] T. Ishizaki, Q. Xu, T. Yoshiie, S. Nagata, *Mater. Trans.* **45** (2004) 9.
[14] T. Iwai, Y. Ito, M. Koshimizu, *J. Nucl. Mater.* **329** (2004) 963.
[15] R. Sugano, K. Morishita, A. Kimura, *Fusion Sci. Technol.* **44** (2003) 446.
[16] R. Vassen, H. Trinkaus, P. Jung, *Phys. Rev. B* **44** (1991) 4206.
[17] D. H. Xu, B. D. Wirth, *Fusion Sci. Technol.* **56** (2009) 1064.
[18] D. H. Xu, B. D. Wirth, *J. Nucl. Mater.* **403** (2010) 184.
[19] C. Domain, C. S. Becquart, *J. Foct, Phys. Rev. B* **69** (2004) 144112.
[20] C. J. Först, J. Slycke, K. J. Van Vliet, S. Yip, *Phys. Rev. Lett.* **96** (2006) 175501.
[21] D. H. Xu, T. Bus, S. C. Glade, B. D. Wirth, *J. Nucl. Mater.* **367** (2007) 483.
[22] D. H. Xu, B. D. Wirth, *J. Nucl. Mater.* **386** (2009) 395.
[23] A. Hardouin-Duparc, A. Barbu, *Mater. Res. Soc. Symp. Proc.* **439** (1997) 509.
[24] M. Kiritani, *Ultramicroscopy* **39** (1991)135.
[25] S. Takaki, J. Fuss, H. K. U. Dedek, H. Schultz, *Radiat. Eff.* **79** (1983) 87.
[26] M. Eldrup, B. N. Singh, *J. Nucl. Mater.* **251** (1997) 132.
[27] T. Troev, E. Popov, P. Staikov, N. Nankov, *Phys. Status Solidi C 6* **11** (2009) 2373.